Title

Transcriptomic analysis reveals that BMP4 sensitizes glioblastoma tumor-initiating cells to mechanical cues

Authors

Hughes, Jasmine H
Ewy, Jeanette M
Chen, Joseph
et al.

Publication Date

2020

DOI

10.1016/j.matbio.2019.06.002

Peer reviewed

Published in final edited form as:

Matrix Biol. 2020 January ; 85-86: 112–127. doi:10.1016/j.matbio.2019.06.002.

Transcriptomic analysis reveals that BMP4 sensitizes glioblastoma tumor-initiating cells to mechanical cues

Jasmine H. Hughes[1,3], **Jeanette M. Ewy**[2,3], **Joseph Chen**[3], **Sophie Y. Wong**[1,3], **Kevin M. Tharp**[4], **Andreas Stahl**[1,5], **Sanjay Kumar**[1,3,6,*]

[1]UC Berkeley - UCSF Graduate Program in Bioengineering, University of California, Berkeley, Berkeley, CA 94720, USA

[2]Department of Molecular and Cell Biology, University of California, Berkeley, Berkeley, CA 94720, USA

[3]Department of Bioengineering, University of California, Berkeley, Berkeley, CA 94720, USA

[4]Center for Bioengineering and Tissue Regeneration, Department of Surgery, University of California San Francisco, San Francisco, CA 94720, USA

[5]Department of Nutritional Sciences and Toxicology, University of California, Berkeley, Berkeley, CA 94720, USA

[6]Department of Chemical and Biomolecular Engineering, University of California, Berkeley, Berkeley, CA 94720, USA

Abstract

The poor prognosis of glioblastoma (GBM) is associated with a highly invasive stem-like subpopulation of tumor-initiating cells (TICs), which drive recurrence and contribute to intratumoral heterogeneity through differentiation. These TICs are better able to escape extracellular matrix-imposed mechanical restrictions on invasion than their more differentiated progeny, and sensitization of TICs to extracellular matrix mechanics extends survival in preclinical models of GBM. However, little is known about the molecular basis of the relationship between TIC differentiation and mechanotransduction. Here we explore this relationship through a combination of transcriptomic analysis and studies with defined-stiffness matrices. We show that TIC differentiation induced by bone morphogenetic protein 4 (BMP4) suppresses expression of proteins relevant to extracellular matrix signaling and sensitizes TIC spreading to matrix stiffness. Moreover, our findings point towards a previously unappreciated connection between BMP4-induced differentiation, mechanotransduction, and metabolism. Notably, stiffness and

*To whom correspondence should be addressed.

7.Author Contributions

J.H.H., S.Y.W. and S.K. designed the study. J.H.H., J.C., J.M.E., S.Y.W., K.M.T. acquired data. J.H.H., J.C., J.M.E., K.M.T., A.S., S.K. analyzed and interpreted the data. J.H.H., S.K. drafted the manuscript with input and approval from all other authors.

5.Conflicts of Interest

The authors declare that they have no conflict of interest.

differentiation modulate oxygen consumption, and inhibition of oxidative phosphorylation influences cell spreading in a stiffness- and differentiation-dependent manner. Our work integrates bioinformatic analysis with targeted molecular measurements and perturbations to yield new insight into how morphogen-induced differentiation influences how GBM TICs process mechanical inputs.

Keywords

mechanotransduction; glioblastoma; bone morphogenetic protein; oxidative phosphorylation; metabolism; stem cell

1. Introduction

Glioblastoma (GBM) is the most common and most lethal primary brain cancer. Difficulty in treating this disease has been attributed to a rare but important subpopulation of cells that evade chemotherapeutic treatment, diffusely invade the surrounding tissue, and establish secondary tumors (1–3). These tumor-initiating cells (TICs) share characteristics with neural stem cells (NSCs) in that they self-renew, express high levels of common molecular markers (e.g., SOX2, nestin), and are isolated from tissue by neurosphere suspension culture (4, 5). Like NSCs, GBM TICs are multipotent, differentiating in response to morphogens to produce cells expressing neural, oligodendrocytic and astrocytic markers. Through the process of self-renewal and differentiation, TICs and their progeny contribute significantly to the heterogeneous cell populations that make up the bulk of the tumor (6–8). Indeed, GBMs frequently arise in brain regions associated with adult NSC populations, suggesting that many GBMs may originate from NSCs that have acquired oncogenic mutations (8–10).

Mechanical and biophysical cues have become increasingly accepted as important factors in tumor progression and metastasis (11, 12) and in stem cell self-renewal (13, 14). In recent years, attention has turned to how these mechanobiological cues govern TIC self-renewal, invasion, and tumor-initiating capacity (15–18). Interestingly, in contrast to the vast majority of cell types, some GBM TICs show reduced sensitivity to mechanical cues. For instance, rather than showing the characteristic rounded cell morphologies and reduced migration speeds on soft substrates, many TICs are able to spread and migrate equally well on a wide range of substrate stiffnesses. Furthermore, this lack of mechanosensitivity is associated with increased invasive potential (19–21).

There is accumulating evidence that TIC stem-like state, mechanical signaling, and invasive capacity are closely intertwined. First, mechanical cues influence TIC self-renewing capacity and stem marker expression (17, 22). Second, perturbations of cytoskeletal signaling in GBM TICs are associated with increased invasiveness. For example, several integrins, which directly link cells to the surrounding extracellular matrix (ECM), have been identified as overexpressed in GBM TICs and have been demonstrated to play key roles in invasion and self-renewal (21, 23–25). Stem-like breast cancer cells show increased myosin IIB expression compared to genetically-matched differentiated breast cancer cells, allowing improved invasion through small pores (26). Similarly, GBM TICs show upregulated Rho GTPase activity compared to less invasive genetically matched bulk tumor cells (21). Third,

invasive capacity in GBM cells is correlated with enriched expression of markers commonly associated with stem cells, including SOX2 (27), CD44 (28) and nestin (29).

In a recent study, we showed that patient-derived GBM TICs demonstrate surprisingly little sensitivity to ECM mechanical cues (20). These cells do not exhibit the rounded morphologies and reduced migration speeds seen in continuous GBM cell lines cultured on very soft substrates (30). However, constitutively activating actomyosin contractile forces sensitized these cells to matrix stiffness, and greatly inhibited their ability to invade *in vitro* and *in vivo.* These responses could also be partially restored by treatment with bone morphogenetic protein 4 (BMP4), which sensitized cell spreading to ECM stiffness. More broadly, BMP proteins have arisen as morphogens of interest in GBM TICs due to the crucial instructive role they play in the adult NSC niche (7, 31). BMP4 has been found to inhibit tumor-initiating capacity as well as induce expression of differentiation markers in TICs (7). Thus, an important open question raised by our study is the molecular basis of the relationship between lack of sensitivity to ECM mechanical cues and morphogen-induced differentiation processes. Understanding the roles differentiation and mechanosensitivity play in TIC signaling would advance our knowledge of tumor progression and may serve therapeutic purposes.

In this study, we investigate connections between stemness and mechanosensitivity in GBM TICs by using a combination of RNA sequencing, bioinformatics analysis, and cell culture studies. Throughout, we validate that stiffness- and BMP4-modulated transcripts are also enriched at the level of protein expression. While changes in ECM stiffness intrinsically alter expression of a relatively limited subset of genes, this number is greatly broadened by treatment with BMP4. Interestingly, the set of mechanically-regulated genes is strongly enriched in genes relevant to ribosome function and oxidative phosphorylation. We also show for the first time that inhibition of oxidative phosphorylation alters cell spreading and oxygen consumption rates in a differentiation- and stiffness-dependent manner. To our knowledge, this is the first report of mechanical regulation of metabolic machinery in GBM TICs, providing insight on how the microenvironment could regulate cellular responses to therapeutics that target energy production.

2. Results

2.1 BMP4 sensitizes cell spreading and nuclear translocation of mechanotransductive signaling factors to matrix stiffness

As described earlier, we had previously shown that the spreading and invasion of GBM TICs are comparatively insensitive to stiffness cues. When treated with BMP4, these cells show an increase in neural differentiation markers such as glial fibrillary acidic protein (GFAP) (Figure 1A, and (20)). This pro-differentiation effect also sensitizes these cells to stiffness-induced changes in cell spreading (Figure 1B–C, conducted on PA gels conjugated with laminin using 2PCA-based N-terminal conjugation; results are qualitatively similar to PA conjugated with laminin via side-chain lysines (20)). TICs cultured in growth factor-enriched self-renewal medium (+GF) did not show a difference in cell spreading area between soft gels and stiff gels ($p = 0.96$). BMP4-treated cells had significantly smaller

areas than control cells and showed a further 18% reduction in median cell area on soft gels compared to stiff gels (Figure 1B–C).

Having reestablished our earlier finding, we next asked whether these morphological changes were accompanied by the activation of canonical signals associated with mechanotransduction. The transcriptional coactivators YAP (Yes-associated protein) and TAZ (transcriptional coactivator with PDZ-binding motif, also known as WW domain-containing transcription regulator protein 1, or WWTR1), have been identified as key mediators of mechanotransduction. Specifically, matrix stiffening induces YAP/TAZ to translocate from the cytoplasm to the nucleus, where they engage specific cofactors to modulate gene expression (32, 33). We therefore hypothesized that BMP4 treatment may enhance nuclear mobilization of TAZ on stiff ECMs. Indeed, we found that there was no statistically significant difference between control cells grown on either soft or stiff gels or BMP4-treated cells on soft gels, but that BMP4-treated cells on stiff gels showed a 22% increase in median nuclear localization of TAZ compared to BMP4-treated cells on soft gels (Figure 1D–E).

2.2 BMP4 influences a broader subset of transcripts than matrix stiffness and increases the number of stiffness-sensitive genes

The results above suggest that BMP4-mediated signaling and mechanotransductive signaling interact in complex ways. To gain a more comprehensive molecular picture of mechanisms that might define these connections, we applied whole-genome RNA sequencing to TICs exposed to soft or stiff substrates, with or without BMP4 treatment. BMP4 elicited a pronounced effect on the transcriptome, consistent with the pro-differentiation effect of BMP4 on TICs (Figure 2A, left two panels). BMP4 treatment altered expression (FDR < 0.05, fold-change > 2) of 2243 named genes on soft matrices (downregulated 1124, upregulated 1119) and 1905 named genes on stiff matrices (958 downregulated, 947 upregulated) in comparison to stiffness-matched GF-treated controls. Most of the genes influenced by BMP4 treatment were common to cells on both matrix conditions (1540 genes in common), although 365 genes and 703 genes were unique to cells differentiated on stiff gels and soft gels respectively (Figure 2B).

In comparison with BMP4 treatment, substrate stiffness impacted the transcriptome to a relatively modest degree (Figure 2A, right two panels). Just 30 genes were significantly (FDR < 0.05) differentially expressed with a fold change greater than two across soft gels and stiff gels for cells cultured in GF-enriched media (22 genes upregulated and 8 genes downregulated by high stiffness). For BMP4-treated cells, this figure was higher by 80%; 54 genes were differentially expressed between cells grown on soft gels versus stiff gels (40 genes upregulated and 14 genes downregulated by high stiffness). Just one gene (C4orf48) showed >2 fold change in both media conditions (FDR < 0.05; Figure 2C). All named genes differentially expressed (FDR < 0.05) across soft and stiff gels are shown in Figure 2D. The 35 genes common to both media conditions were largely expressed at higher levels on stiff substrates compared to soft, although two genes (AGT and EMP1) showed a switch in the directionality of their mechanosensitivity (Figure 2D).

BMP4 treatment alters the transcriptome to a much larger extent than a change in stiffness does. This finding is consistent with the broad phenotypic changes associated with differentiation, including alterations in cell morphology, marker expression, and functional maturation. Our transcriptomic findings are also consistent with three observations from our earlier work (20): first, the distribution of marker-positive progeny in response to BMP4 treatment does not depend strongly on matrix stiffness, implying that stiffness does not bias or instruct differentiation. Second, undifferentiated TICs are largely insensitive to mechanical cues (20). Third, BMP4 sensitizes these cells to substrate stiffness.

2.3 Pathway analysis reveals BMP4 downregulates signaling associated with ECM interaction

To better understand how BMP4 alters gene expression, we next mined our RNAseq data to identify signaling systems that might be preferentially impacted by BMP4 expression compared to stiffness-matched controls. We found that BMP4 significantly upregulated genes associated with axon guidance, such as ephrins, ephrin receptors, and several semaphorins (Figure 3A, Supplementary Figure 1). We also found that BMP4 suppressed PI3K-Akt signaling, including downregulation of MAP2Kl (MEK1) (Supplementary Figure 1). Both findings are consistent with BMP4's observed pro-differentiation and anti-proliferative effects on TICs (7). BMP4 treatment also downregulated genes associated with ECM-receptor interactions, focal adhesions and proteoglycans, such as many integrin subunits, zyxin, paxillin and CD44 (Supplementary Figure 1).

Our findings support at a more systems-level past reports that identified integrins, RhoGTPases and myosin II as distinguishing more invasive or more stem-like TICs from less invasive or more differentiated TICs (21, 23–26). BMP4 treatment strongly inhibited the expression of the actomyosin force generation activators myosin light chain 12A (MYL12A) and ROCK2, which is somewhat surprising given that we had shown that activation of the actomyosin contractility sensitized this TIC line to mechanical cues. However, others have associated increased RhoA and NMII activity with greater propensity for invasion in GBM cells (21, 26). Furthermore, mechanotransduction is also strongly regulated by posttranslational modification, subcellular localization, and other factors, which may collectively render the relationship between gene expression and signaling activity markedly nonlinear (34, 35).

2.4 BMP4 elicits a pro-differentiation effect at the transcriptional level

Several investigators have reported transcriptional or proteomic changes in specific markers in GBM TICs treated with BMP4 or have identified specific markers associated with TIC sternness (7, 36). Consistent with these reports, we found BMP4 upregulated expression of the neural marker βIII tubulin (TUBB3) and the astrocytic marker GFAP (Fig 3B). We did not observe an appreciable change in expression of the oligodendrocyte marker galactosylceramidase (GALC), consistent with the findings by Piccirillo and colleagues that this lineage was the least commonly produced by BMP4-treated TICs (7). Of the core four transcription factors that have been reported to drive GBM propagation (36), two (OLIG2, POU3F2) were significantly downregulated by BMP4 treatment, one (SALL2) was upregulated by BMP4 treatment and one (SOX2) was not impacted by BMP4 treatment. A

BMP4-dependent increase in SALL2 expression may reflect its somewhat mixed pro-tumorigenic and tumor-suppressive effects (37–39).

2.5 Substrate stiffness regulates expression of ribosomal protein and oxidative phosphorylation genes

To determine how substrate stiffness alters the transcriptomic profile of these TICs, we next performed pathway analysis on the list of genes differentially expressed (FDR < 0.05) in cells grown on different stiffness conditions in media supplemented with either GFs (Figure 3C) or BMP4 (Figure 3D). Interestingly, while few genes are differentially expressed across different gel stiffness conditions in both media conditions, changes in substrate stiffness produced similar transcriptomic changes in both BMP4-treated and GF-treated cells at the pathway level. Somewhat unexpectedly, these conserved pathways included ribosome proteins and oxidative phosphorylation (OXPHOS). Moreover, deeper inspection of the other gene sets (e.g. Parkinson's Disease, Cardiac Muscle Contraction) reveals that the differentially expressed genes in these sets overlap almost entirely with oxidative phosphorylation (Figure 3E). While changes in substrate stiffness influenced the expression of a different a subset of genes for each media condition (Figure 3E, light blue (+GF) and dark blue (+BMP4)), some genes were stiffness-sensitive under both media conditions (Figure 3E, orange). We then examined how single genes within each set change with stiffness in each medium condition (Fig. 3F). Ribosome protein expression is upregulated by both BMP4 treatment and by matrix stiffening (Figure 3F, orange points). OXPHOS genes follow a more mixed picture; although BMP4 upregulates a few OXPHOS genes its net effect is to downregulate OXPHOS genes, while stiffness universally upregulates OXPHOS genes (Figure 3F, blue points).

2.6 Transcriptional response to matrix stiffness cannot be fully explained by canonical mechanotransductive transcription factors

Given that matrix stiffening induces TAZ nuclear translocation in BMP4-treated TICs (Fig. 1), and given the demonstrated importance of YAP and TAZ in mediating mechanotransduction, we wondered if YAP/TAZ targets might be differentially expressed across different stiffness conditions in our cells. Surprisingly, relatively few previously identified YAP/TAZ targets (32, 40) changed expression as a function of stiffness (Figure 3G). Instead, cells grown in GF-enriched media, which largely do not respond to differences in mechanical cues, showed a significantly (Pearson's χ^2 p value < 0.05) higher proportion of stiffness-altered genes that were targets of YAP/TAZ (9 of 171 named stiffness-sensitive genes, FDR < 0.05) compared to the BMP4-treated cells (8 of 466 171 named stiffness-sensitive genes, FDR < 0.05). This finding highlights that other transcription factor(s) are also important in the transcriptomic response of these cells to mechanical cues, either independently or in concert with YAP/TAZ signaling.

2.7 RNA sequencing predictions confirmed at mRNA and protein level

To validate our transcriptomic data is predictive of protein expression, we identified a short list of protein targets that were associated with one or more of the KEGG pathways (Figure 3 and Supplementary Figure 1). We ultimately selected mitogen-activated protein kinase kinase (MAP2K1, also known as MEK1), α-actinin-l (ACTN1), TAZ and zyxin (ZYX) for

their strongly validated roles in mediating mechanotransductive signals (Figure 4A). Each of the targets probed showed a significant change in expression in the predicted direction (Figure 4B–C). To our knowledge, these findings are the first evidence that these mediators of mechanotransduction alter during BMP4-induced differentiation. Our observation that TAZ decreases in expression after BMP4 treatment is consistent with our finding that YAP/TAZ target genes are not strongly differentially expressed across different substrate stiffnesses in BMP4-treated cells.

Integrin signaling has been previously observed to be upregulated in patient tumor samples compared to normal brain (25). At the transcriptomic level, we observed significantly higher expression of integrin subunits in TICs cultured in GF-enriched medium relative to those treated with BMP4 (Figure 3A; Supplementary Figure 1F). The one exception was Integrin α_2 (ITGA2), which instead shows a large increase in expression following BMP4 treatment. ITGA2 complexes exclusively with Integrin β_1 (ITGB1) and binds collagen, laminin and E-Cadherin (CDH1) (41). While several integrins have received close attention in the context of GBM cancer stem cells (23, 24), comparatively less is known about ITGA2. Some evidence indicates ITGA2 is lower in breast cancer cells compared to healthy tissue and decreased ITGA2 is associated with increased invasiveness and poorer prognosis (42–44).

Interestingly, we discovered that the α_2 subunit is also upregulated by BMP4 at the transcriptional level (Figure 4D) and at the protein level (Figure 4E). ITGA2 signal in TICs cultured in GF-enriched medium was mostly diffusely cytoplasmic. Increased localization of ITGA2 was observed at cell peripheries and at cell-cell contacts in BMP4-treated cells cultured on stiff gels compared to those on soft gels (Figure 4F), suggesting ITGA2 may be playing a role in adhesion and mechanotransduction. As previously described, these cells do not exhibit well-defined focal adhesions (20), precluding meaningful co-localization of ITGA2 with other focal adhesion proteins.

As further validation of our RNA sequencing predictions, we tested the expression of four genes with reverse transcription polymerase chain reaction (rt-PCR), selecting the OXPHOS proteins NADH dehydrogenase:ubiquinone 1 alpha subcomplex subunit 2 (NDUFA2), Cytochrome c oxidase polypeptide 7A2 (COX7A2), TAZ and the YAP/TAZ target endothelial plasminogen activator inhibitor-1 (SERPINE1) for their predicted mechanosensitivity (Figure 4H–I). While COX7A and SERPINE1 showed the expected upregulation on stiff gels compared to soft gels for cells grown in GF-enriched media, trends in NDUFA2 and TAZ were considerably more muted. Although trends were often as expected, with this limited sample size, differences across media conditions were not significant for TAZ and differences across stiffness conditions were not significant for NDUFA2. The lack of an exact agreement between RNASeq and rt-qPCR is perhaps not surprising given differences in the inherent biases and statistical power across the two methods (45).

2.8 Inhibition of oxidative phosphorylation impacts oxygen consumption and cell spreading in a stiffness- and differentiation state-dependent manner

Because of the surprising enrichment of OXPHOS in the genes regulated by stiffness, we wondered if metabolic rates were altered by stiffness in these cells. We measured oxygen

consumption rates (OCR), and found that under self-renewing conditions, oxidative phosphorylation rates were indeed influenced by substrate stiffness, with soft matrices suppressing OCR by 30% compared to the stiff condition (Figure 5A). BMP4 treatment severely reduced oxygen consumption on both soft and stiff substrates, overwhelming any secondary effect of matrix stiffness.

We next asked if inhibiting OXPHOS would influence the ability of cells to spread, as an indicator of ability to communicate mechanical ECM properties and extend processes. We treated the cells with 5 μM oligomycin, an ATP synthase inhibitor that prevents conversion of ADP to ATP through OXPHOS (46). Over the course of 30 minutes we observed that GF-treated TICs showed a noticeable retraction of protrusions (Figure 5B, left; white arrows). This change in cell spreading was particularly dramatic for the GF-treated TICs on stiff gels, where some cells became much more rounded and sometimes collapsed into clusters of cells. In contrast, BMP4-treated cells showed lower levels of protrusion retraction and indeed often showed protrusion extension (Figure 5B, right; yellow arrows). Quantification of cell area before and after oligomycin addition (Figure 5C) demonstrated that while GF-treated TICs became less spread, the BMP4-treated cells were able to spread in the presence of oligomycin. For the GF-treated TICs, this change in cell area was stiffness-dependent, with the cells on soft gels decreasing in area by a median of 8.7% while the cells on stiff gels decreased in area by a median of 17.8%. This finding is consistent with our RNA sequencing data, in which oxidative phosphorylation was upregulated on stiff substrates. While we had expected to see more of a difference in the BMP4-treated cells, the lack of effect seen is likely due to their significantly lower OCR. Indeed, this finding is consistent with the BMP4's suppressive effect on PI3K signaling (Figure 3A), which is known to influence metabolism and decrease oxygen consumption (47, 48). Together, these results highlight the relationship between differentiation and metabolism, and provides new evidence of the regulation of metabolism by matrix stiffness.

3. Discussion

Increasing evidence suggests that stem-like GBM TICs show reduced sensitivity to mechanical cues and heightened invasive potential. One facet that remained unclear is how differentiation of TICs alters their ability to sense and respond to their mechanical environment. We show here that BMP4 elicits a pro-differentiation effect that sensitizes cell spreading and nuclear translocation of TAZ to substrate stiffness. Through RNA sequencing, we discovered that BMP4 down-regulates a broad set of genes associated with ECM adhesion-dependent signaling. We also found that stiffness cues regulate expression of ribosome proteins and oxidative phosphorylation proteins regardless of differentiation state, but that BMP4-mediated differentiation increases the number of genes differentially expressed across different matrix stiffness conditions. We observed a strong decrease in oxidative phosphorylation upon BMP4 treatment, with stem-like cells showing higher oxygen consumption rates on stiffer substrates. Through inhibition of oxidative phosphorylation, we show that cell spreading depends on oxidative phosphorylation in a stiffness- and differentiation-dependent manner.

Increasing attention has been paid to the dysregulation of mitochondria and metabolism in cancer, and these efforts have shed considerable light into how mitochondrial signaling regulates proliferation, survival and response to chemotherapy (49). We show here that transcription of oxidative phosphorylation genes is suppressed by BMP4 treatment and by soft substrates, and that functional measurements of basal oxygen consumption rates corroborate this finding. This finding mirrors prior work that found glioma stem cells (50) and other cancer stem cells (51) rely less on glycolysis than their more differentiated counterparts. The role that the mechanical microenvironment plays in modulating the function of mitochondria, which are anchored to the cytoskeleton, is only beginning to be investigated (52). Recent studies have demonstrated that metabolic parameters can be strongly influenced by ECM physical properties such stiffness and fiber alignment. For example, the ATP:ADP ratio in migrating cells is higher in dense matrices or when cytoskeletal force generation is inhibited, and lower in aligned matrices where migration is facilitated (53). Basal metabolic rates are higher on stiff substrates, and both stiffness and fiber alignment modulate cellular responses to metabolic stress (54). Metabolism also appears to be coupled to forces transmitted through the actin cytoskeleton and through cell-cell adhesions (55, 56). The link between ECM mechanics and transcriptional modulation of mitochondrial function is less clear. We recently showed that actomyosin-mediated YAP/TAZ signaling regulates uncoupled respiration in brown adipose tissue (57). Our transcriptional data further support a role for stiffness in transcriptional regulation of oxidative phosphorylation. While blocking oxidative phosphorylation has been shown to impact cell shape (58), to our knowledge this is the first evidence that stiffness modulates this relationship.

A challenge in studying the differentiation of TICs is their epigenetic plasticity, which allows them to revert to more stem-like states after differentiation by culturing in supraphysiological levels of growth factors (59–62). In particular, there is some evidence that SOX2 mediates this plasticity, with SOX2 knockout inhibiting de-differentiation of GBM cancer stem cells (60) and incomplete chromatin remodeling observed at sites with SOX binding motifs even after differentiation (59). It is therefore interesting that we do not observe changes in SOX2 expression between differentiated and undifferentiated cells. One intriguing question is whether de-differentiated TICs regain mechanosensitivity along with re-entry of the cell cycle.

Although we found that stiffness-induced TAZ localization is heightened in BMP4-treated cells, we were surprised to find there is little overlap between the genes we identify here as mechanically regulated and previously validated YAP/TAZ target genes (32, 40). This finding is consistent with a growing number of studies from our own lab (63) and others (64) indicating that YAP and TAZ do not always play functionally important transcriptional co-activation roles in response to matrix stiffening. Also unexpected was the finding that rather than simply amplifying the number of genes that are differentially expressed, BMP4-treatment eliminates the mechanoresponsiveness of some genes while sensitizing other genes to mechanical cues. Together, these findings emphasize that mechanical regulation of transcription goes beyond YAP and TAZ, either by the modulation of the activity of these co-activators by other transcription factors or via additional presently unidentified mechanosensitive transcription factors acting independent of YAP/TAZ.

Overall, our work demonstrates that BMP4's pro-differentiation effect sensitizes GBM TICs to substrate stiffness, and hints towards the importance of the mechanical microenvironment in regulating metabolism and ribosome biogenesis. Since tumors often have different mechanical properties than surrounding tissue (65, 66), this work may help shed light on heterogeneous responses to chemotherapeutics targeting metabolic pathways. It will be important to determine whether the findings here generalize across TICs derived from a wide range of GBMs of varying subtype and clinical presentations and assess the patient-to-patient variability in this phenotype. Indeed, both GBM TIC mechanosensitivity and metabolism show considerable inter-individual variablity (19, 67). Nevertheless, this interplay between environmental stiffness cues and GBM TIC metabolism will be an intriguing new direction. In future work, it will be valuable to identify transcription factor interactions that could integrate mechanical signals to regulate genes associated with oxidative phosphorylation.

4. Methods

4.1 Tumor-initiating cell culture

The L0 patient-derived classical subtype tumor-initiating cells were a kind gift from Professor Brent Reynolds (4) and were further characterized by our labs in a recent publication (20). Cells were cultured in Neurocult (Stem Cell Technologies, 05751) supplemented with 20 ng/ml epidermal growth factor (EGF; Peprotech, 236-EG-200) and 10 ng/ml fibroblast growth factor (FGF; R&D Systems 233-FB-025/CF). Under these conditions, TICs grow in suspended neurospheres, which were serially passaged every 5-7 days by dissociation with 0.05% trypsin/ethylenediaminetetraacetic acid for 2 min at 37°C followed by quenching in trypsin inhibitor. All experiments were conducted with cells passaged fewer than twenty times. For BMP4 treatment, cells were cultured in Neurocult supplemented with 100 ng/ml BMP4 (R&D Systems, 314-BP-010/CF). Control cells were cultured in Neurocult supplemented with 10 ng/ml FGF and 20 ng/ml EGF.

4.2 Polyacrylamide gel synthesis

Polyacrylamide (PA) gels of "soft" (100-250 Pa) and "stiff" (40-60 kPa) elastic moduli were synthesized and functionalized with laminin via the cross-linker Sulfo-SANPAH for RNA extraction and functionalized with laminin via 2-pyridinecarboxaldehyde (2PCA) for all other assays as described previously (68). Briefly, acrylamide (A) and N-N'-methylene-bis-acrylamide (B) were mixed at 3%A/0.04%B (soft) and 15%A/1.2%B (stiff) and dissolved oxygen was removed by bubbling with nitrogen gas. For gels functionalized with 2PCA, 2PCA was added directly to the acrylamide/bis solution at a 0.1% mole fraction relative to acrylamide monomer content. The gels were polymerized with ammonium persulfate (Bio-Rad, 10% w/v stock made in ultrapure water, to a final concentration of 0.1%) and tetramethylethylenediamine (Bio-Rad, 0.1% v/v) while sandwiched between a glass coverslip activated with bind-silane (Sigma Aldrich, GE17-1330-01) and a glass slide treated with water repellent (Rain-X). After 30 minutes, the hydrophobic glass slide was removed from the polymerized gels. Gels functionalized with Sulfo-SANPAH were submerged in Sulfo-SANPAH (ThermoFischer Scientific, 22589) for 8 minutes under a UV lamp and then rinsed twice in PBS. Regardless of functionalization method, gels were then incubated in 0.1

mg/mL laminin (Invitrogen, 23017-015, isolated from mouse Engelbreth-Holm-Swarm tumor) overnight at 37°C.

4.3 Flow Cytometry for Validation of Differentiation

Cells were seeded at 30,000 cells/cm^2 on tissue culture plastic that had been coated overnight at 4°C in 0.1 mg/mL laminin, and cultured for two days in either growth-factor enriched medium or BMP4-supplemented medium. Cells were incubated for 5 min. at room temperature in accutase (Innovative Cell Technologies, AT104) to form a cell suspension, then pelleted and fixed in 2% PFA/1% bovine serum albumin (BSA: Sigma Aldrich, A9647) diluted in Dulbecco's PBS.

Fixed cells were blocked and permeabilized in a staining buffer made from 1 mg/ml saponin (Sigma Aldrich, 47036) in 5% goat serum and 1% BSA for 15 minutes, then stained with anti-GFAP (Cell Signalling, 80788, produced in rabbit) diluted 1:25 in the staining buffer for one hour at room temperature. Samples were washed twice in staining buffer, then stained for one hour in the dark in 1:100 goat anti-rabbit Alexa Fluor 488 conjugate (Thermo Fisher Scientific, A-11008) and 1:400 DAPI in staining buffer. Samples were washed twice in 1% goat serum in PBS, and analyzed on an Attune flow cytometer (Thermo Fischer). Measurements were gated according to DAPI intensity, forward scatter and side scatter, and GFAP signal was assessed relative to the intensity of a sample incubated without primary antibodies. Experiment was performed thrice and a representative curve is shown.

4.4 Cell Area Measurements

Cells were seeded at 10,000 cells/cm^2 on PA gels functionalized with laminin via 2PCA and cultured in BMP4- or GF-supplemented media for 2 days. For ATP synthase inhibition, a solution of media and oligomycin (EMD Millipore, 495455) was added to the culture media to a final concentration of 5 μM, and cells were imaged before treatment and 30 minutes after treatment. Phase contrast images were taken with a Nikon TE2000-E2 microscope and the perimeter of the cells were manually traced on ImageJ to calculate the cell area. Cells were excluded from analysis if >5% of the cell perimeter was in contact with another cell.

4.5 Immunocytochemistry

Cells were seeded at 10,000 cells/cm^2 on 2PCA-functionalized PA gels and cultured in BMP4- or GF-supplemented media for 7 days. Cells were fixed in 4% paraformaldehyde (PFA; Fisher Scientific, #30525-89-4) in Dulbecco's PBS (Sigma-Aldrich, D1283) for 10 minutes. The samples were treated with 0.1% sodium borohydride (Spectrum Chemical, S1187) for 10 minutes to reduce nonspecific antibody binding with the PA gels, then permeabilized with 0.5% Triton-X100 (EMD Millipore, 9410) for 12 minutes. Samples were blocked with 5% goat serum (GS; Thermo Fisher Scientific, 16210064) for at least 1 hour then incubated overnight in primary antibodies diluted in 1% GS at 4°C. Samples were then washed in 1% GS and stained in secondary antibodies and 1: 400 DAPI (Sigma-Aldrich, 10236276001) diluted in 1% GS for 1 hr at room temperature. The following antibodies and dilutions were used: 1:100 anti-TAZ clone M2-616 (produced in mouse, BD Biosciences, 560235), 1:100 anti-ITGA2 (produced in mouse, Abcam, abl0800), 1:200 goat anti-mouse Alexa Fluor 647 conjugate (Thermo Fisher Scientific, A21235). Samples were then washed

in 1% GS then in PBS. Representative images have background signal subtracted for display purposes.

4.6 Nuclear Localization of TAZ

Epifluorescent images of cells probed for TAZ (WWTR1) were taken with a Nikon TE2000-E2 microscope equipped with a 20X objective. Image analysis was performed using ImageJ (NIH)(69). TAZ images were overlaid with DAPI stains and background was subtracted. The DAPI channel was used to create a mask of the nucleus and nuclear intensity of TAZ was divide by the total background-subtracted intensity of TAZ. Nuclear localization is calculated per field of view, with each image containing 5-20 individual cells. Due to the 1-week culture period, cells often overlapped too much to allow segmentation of individual cells.

4.7 RNA Sequencing Sample Preparation

Cells were seeded at 20,000 cells/cm^2 on PA gels functionalized with laminin via Sulfo-SANPAH. BMP4-treated cells were cultured for 7 days while untreated cells were cultured for 3 days due to their more rapid growth and arrival at confluence. Cells were lysed with TRIzol reagent (Life Technologies, 15596026) and RNA was extracted using the RNeasy Micro Kit (Qiagen, 74004) according to the manufacturer's protocol. Duplicate samples were collected in two distinct experiments with cells of separate passage numbers. Total RNA samples were submitted to the University of California, Berkeley QB3 Functional Genomics Laboratory (FGL) for sequencing preparation. Total RNA was checked on a Bioanalyzer (Agilent) for quality, and only high-quality RNA samples (RIN > 8) were used. At the FGL, Oligo $(dT)_{25}$ magnetic beads (Thermofisher) were used to enrich mRNA. The treated RNAs were rechecked on Bioanalyzer for integrity. The Library preparation for Alumina sequencing was done on the Apollo 324™ with PrepXTM RNA-Seq Library Preparation Kits (WaferGen Biosystems, Fremont, CA) according to the manufacturer's recommendation. Libraries were then visualized again on the Bioanalyzer and transferred to the UC Berkeley-QB3 Vincent J. Coates Genomics Sequencing Laboratory where they were qualified by real-time PCR on a Roche Lightcycler 480II (Roche Applied Biosciences, Indianapolis, IN) with Kapa Biosystems Illumina quantification reagents (Kapa biosystems, Wilbur, MA). Libraries were then pooled in equimolar ratios and sequenced on the Illumina HiSeq2000 in High Output Mode using v3 single-end 50 base-pair chemistry (Illumina Inc., San Diego, CA).

4.8 RNA Sequencing Analysis

Read quality was assessed using FastQC (70) and Phred scores were found to be greater than 28. Low quality ends and adaptor sequences were removed using the FASTQ Trimmer and FASTQ Clipper. Sequences were aligned to the human reference genome GRCh38 using TopHat2 (71) and differential expression analysis was conducted with the Cufflinks package version 2.1 (72). Cufflinks determines statistical significance by sampling from the beta negative binomial. The default number of simulations were used, and therefore the minimum p-value reported is 10^{-5}. Data is available upon request.

4.9 Pathway Enrichment Analysis

DAVID Bioinformatics Resources version 6.8 (2016) (73) was queried with gene lists of interest to determine Kyoto Encyclopedia of Genes and Genome (KEGG) pathway enrichment. Briefly, a modified Fisher's Exact p-value (EASE score) is calculated with the null hypothesis being that the number of genes from a list of genes that fall within a specific pathway is equal to the number that would be expected to fall within that pathway due to random chance. This p-value is then corrected for multiple comparisons according to the Benjamini-Hochberg method. For Figure 3A, the two gene lists were the sets of named genes significantly (FDR < 0.05) upregulated (712 genes) or downregulated (608 genes) by BMP4 by a factor of $2^{1.5}$ or higher for stiffness-matched comparisons. For Figure 3C and 3D, the gene lists were the set of 171 or 466 named genes significantly differentially expressed (FDR <0.05) between the two matrix stiffnesses for GF-treated cells or BMP4-treated cells, respectively.

4.10 Real-time Polymerase Chain Reaction

Cells were lysed and homogenized through a 20-gauge needle and total RNA was purified using the RNeasy mini kit (Qiagen, 74104); cDNA was synthesized using cDNA Synthesis SuperMix (Bimake, B24408) following the manufacturers' protocols. Real time PCR was performed with TaqMan Gene Expression Assays (Applied Biosystems) on a BioRad CFX Connect. Taqman primers were purchased: SERPINE1 (Hs00167155_m1), COX7A2 (Hs01652418_m1), NDUFA2 (Hs04187282_g1), TAZ (Hs00902887_g1) and samples were normalized to Ribosomal Protein S9 (RPS9) (Hs02339424_g1).

4.11 Western Blots

Cells were lysed in 1% protease inhibitor cocktail (Cell Signaling Technologies, #5871S), 1% phosphatase inhibitor (EMD Millipore, 524624), 4.1 μg/ml sodium molybdate and 1.4 μg/ml sodium fluoride in radioimmunoprecipitation assay (RIPA) buffer (Sigma-Aldrich, R0278). Protein concentration was measured by bicinchonic acid (BCA) assay (Thermo Fisher Scientific, 23228) according to the manufacturer's specifications and samples were brought to equal protein concentrations with additional lysis buffer. Lysates were mixed with LDS (Thermo Fisher Scientific, NP0007) and reducing agent (Life Technologies, NP0009) and heated at 95 °C for 5 minutes. Samples were run on 4-12% Bis-Tris gels (Life Technologies, NP0323) in MOPS buffer (Life Technologies, NP001) at 170 V for 65 minutes and transferred onto nitrocellulose membranes (LI-COR, 926-31092) at 50 V for 150 minutes in 10% methanol and transfer buffer (Life Technologies, NP0006). Membranes were blocked for at least 1 hour in blocking buffer (LI-COR, 927), then primary antibodies were added and the membranes were incubated overnight at 4°C. Membranes were washed in tris-buffered saline and Tween-20 (TBST), incubated in secondary antibodies diluted in blocking buffer, washed in TBST and imaged on an Odyssey system. The following antibodies were used: anti-cofilin clone D3F9 (Cell Signaling Technologies, 5175), anti-α-actinin-1 (Sigma-Aldrich, A5044), anti-MAP2K1 (Cell Signaling Technologies, 9124), anti-TAZ clone M2-616 (BD Biosciences, 560235), anti-zyxin (Abcam, ab58210), anti-ITGA2 (Abcam, ab133557 or ab10800), IRDye 680RD goat anti-rabbit (LI-COR, 925-68071),

IRDye 800RD goat anti-mouse (LI-COR, 925-32210). Bands were quantified using ImageJ's standard gel analyzer tool, with background signal subtracted.

4.12 Metabolic Measurements

Gels were prepared as described previously on 5 mm glass slides and cells were seeded at 64,000 cells/cm^2 in GF- or BMP4-supplemented media, and cultured for two days. Slides were transferred into Seahorse XF24 islet capture plates (Agilent, 101122-100). Oxygen consumption was measured with the Agilent Seahorse XF24 cellular respirometer. Cells were equilibrated for 30 minutes prior to measurement in XF assay medium with 1 mM pyruvate (Gibco, 11360070), 2 mM glutamine (Gibco, A2916801) and 25 mM glucose. Oxygen consumption rates (OCR) were calculated relative to background measurement reads (2 background wells per condition, 10 technical replicates per condition) and averaged from three subsequent measurements, then normalized to the mean OCR for within-experiment cells grown in GF-supplemented media on stiff gels. Data shown is collected from two independent experiments.

4.13 Statistical Analysis

For the RNA sequencing data, statistical analysis was performed as described above. All other analyses and all graphing were performed in R. Data normality was assessed with the Shapiro-Wilk Normality Test, and datasets where $p < 0.1$ were assessed using non-parametric tests as noted in the figure legends. Unless otherwise noted, experiments were performed independently at least thrice. RNA sequencing samples were collected in duplicate only. Experiments were deemed independent if the gels were made on different days, the cells were passaged and seeded on different days and the assay was conducted on different days.

Supplementary Material

Refer to Web version on PubMed Central for supplementary material.

Acknowledgements

This work used the Vincent J. Coates Genomics Sequencing Laboratory at UC Berkeley, supported by NIH S10 Instrumentation Grants S10RR029668 and S10RR027303. We thank Dr. Mary West of the CIRM/QB3 Shared Stem Cell Facility (SSCF) at UC Berkeley for technical support. Confocal microscopy and flow cytometry were performed in the SSCF. We also thank Bob Lesch and Professor Randy Schekman for the use of their Odyssey, Kelsey Springer for her assistance with rheological measurements, and Professor Valerie M. Weaver for valuable discussions and support of K.M.T. We gratefully acknowledge financial support from the following sources: the Natural Sciences and Engineering Research Council of Canada (NSERC PGS D 555229, J.H.H.), the Siebel Scholars program (J.H.H., S.Y.W.), the W.M. Keck Foundation (S.K.) and the National Institutes of Health (R01GM122375, R21EB025017, S.K.; R01DK118940, S.K. and A.S; F32CA221366, J.C.).

Abbreviations:

TIC	Tumor initiating cell
GBM	glioblastoma
BMP4	bone morphogenetic protein 4

GF	growth factor enriched media
NSC	neural stem cell
OXPHOS	oxidative phosphorylation
FDR	false discovery rate
RNA	ribonucleic acids
RNAseq	RNA sequencing

8. References

1. Chen J, et al. (2012) A restricted cell population propagates glioblastoma growth after chemotherapy. Nature 488. doi:10.1038/nature11287.
2. Nassar D, Blanpain C (2016) Cancer Stem Cells: Basic Concepts and Therapeutic Implications. Annu Rev Pathol Mech Dis 11 (1):47–76.
3. Lathia JD, Mack SC, Mulkearns-Hubert EE, Valentim CLL, Rich JN (2015) Cancer stem cells in glioblastoma. Gems Dev 29(12):1203–17.
4. Deleyrolle LP, et al. (2011) Evidence for label-retaining tumour-initiating cells in human glioblastoma. Brain 134(5): 1331–1343. [PubMed: 21515906]
5. Galli R, et al. (2004) Isolation and Characterization of Tumorigenic, Stem-like Neural Precursors from Human Glioblastoma. Cancer Res 64:7011–7021. [PubMed: 15466194]
6. Lathia JD, et al. (2011) Direct In Vivo Evidence for Tumor Propagation by Glioblastoma Cancer Stem Cells. PLoS One 6(9):e24807. [PubMed: 21961046]
7. Piccirillo SGM, et al. (2006) Bone morphogenetic proteins inhibit the tumorigenic potential of human brain tumour-initiating cells. Nature 444(7120):761–765. [PubMed: 17151667]
8. Lim DA, et al. (2007) Relationship of glioblastoma multiforme to neural stem cell regions predicts invasive and multifocal tumor phenotype. Neuro Oncol 9(4):424–429. [PubMed: 17622647]
9. Sanai N, Alvarez-Buylla A, Berger MS (2005) Neural Stem Cells and the Origin of Gliomas. N Engl J Med 353(8):811–822. [PubMed: 16120861]
10. Quiñones-Hinojosa A, Chaichana K (2007) The human subventricular zone: A source of new cells and a potential source of brain tumors. Exp Neurol 205(2):313–324. [PubMed: 17459377]
11. Paszek MJ, et al. (2005) Tensional homeostasis and the malignant phenotype. Cancer Cell 8(3):241–254. [PubMed: 16169468]
12. Chin LK, Xia Y, Discher DE, Janmey PA (2016) Mechanotransduction in cancer. Curr Opin Chem Eng 11:77–84. [PubMed: 28344926]
13. Saha K, et al. (2008) Substrate Modulus Directs Neural Stem Cell Behavior. Biophys J 95(9):4426–4438. [PubMed: 18658232]
14. Dellatore SM, Garcia AS, Miller WM (2008) Mimicking stem cell niches to increase stem cell expansion. Curr Opin Biotechnol 19(5):534–540. [PubMed: 18725291]
15. Chen J, Kumar S (2017) Biophysical regulation of cancer stem/initiating cells: Implications for disease mechanisms and translation. Curr Opin Biomed Eng 1:87–95. [PubMed: 29082354]
16. Miroshnikova YA, et al. (2016) Tissue mechanics promote IDH1-dependent HIF1α–tenascin C feedback to regulate glioblastoma aggression. Nat Cell Biol 18(12): 1336–1345. [PubMed: 27820599]
17. Tan Y, et al. (2014) Matrix softness regulates plasticity of tumour-repopulating cells via H3K9 demethylation and Sox2 expression. Nat Commun 5:4619. [PubMed: 25099074]
18. Pang M-F, et al. (2016) Tissue Stiffness and Hypoxia Modulate the Integrin-Linked Kinase ILK to Control Breast Cancer Stem-like Cells. Cancer Res 76(18):5277–87. [PubMed: 27503933]
19. Grundy TJ, et al. (2016) Differential response of patient-derived primary glioblastoma cells to environmental stiffness. Sci Rep 6:23353. [PubMed: 26996336]

20. Wong SY, et al. (2015) Constitutive activation of myosin-dependent contractility sensitizes glioma tumor-initiating cells to mechanical inputs and reduces tissue invasion. Cancer Res 75(6): 1113–22. [PubMed: 25634210]
21. Ruiz-Ontañon P, et al. (2013) Cellular plasticity confers migratory and invasive advantages to a population of glioblastoma-initiating cells that infiltrate peritumoral tissue. Stem Cells 31(6): 1075–85. [PubMed: 23401361]
22. Jabbari E, Sarvestani SK, Daneshian L, Moeinzadeh S (2015) Optimum 3D matrix stiffness for maintenance of cancer stem cells is dependent on tissue origin of cancer cells. PLoS One 10(7). doi: 10.1371/journal.pone.0132377.
23. Nakada M, et al. (2013) Integrin α3 is overexpressed in glioma stem-like cells and promotes invasion. Br J Cancer 108(12):2516–2524. [PubMed: 23652300]
24. Lathia JD, et al. (2010) Integrin alpha 6 regulates glioblastoma stem cells. Cell Stem Cell 6(5):421–32. [PubMed: 20452317]
25. Riemenschneider MJ, Mueller W, Betensky RA, Mohapatra G, Louis DN (2005) In Situ Analysis of Integrin and Growth Factor Receptor Signaling Pathways in Human Glioblastomas Suggests Overlapping Relationships with Focal Adhesion Kinase Activation. Am J Pathol 167(5):1379–1387. [PubMed: 16251422]
26. Thomas D, et al. (2016) Increased cancer stem cell invasion is mediated by myosin IIB and nuclear translocation. Oncotarget 7(30):47586–47592. [PubMed: 27285763]
27. Munthe S, et al. (2016) Glioma cells in the tumor periphery have a stem cell phenotype. PLoS One 11(5). doi:10.1371/journal.pone.0155106.
28. Bleau A-M, et al. (2009) PTEN/PI3K/Akt Pathway Regulates the Side Population Phenotype and ABCG2 Activity in Glioma Tumor Stem-like Cells. Cell Stem Cell 4(3):226–235. [PubMed: 19265662]
29. Lin J-MG, et al. (2018) Lab on a Chip Linking invasive motility to protein expression in single tumor cells. 18. doi:10.1039/c71c01008g.
30. Ulrich TA, de Juan Pardo EM, Kumar S (2009) The Mechanical Rigidity of the Extracellular Matrix Regulates the Structure, Motility, and Proliferation of Glioma Cells. Cancer Res 69(10):4167–4174. [PubMed: 19435897]
31. Bond AM, Bhalala OG, Kessler JA (2012) The dynamic role of bone morphogenetic proteins in neural stem cell fate and maturation. Dev Neurobiol 72(7): 1068–1084. [PubMed: 22489086]
32. Dupont S, et al. (2011) Role of YAP/TAZ in mechanotransduction. Nature 474(7350): 179–183. [PubMed: 21654799]
33. Halder G, Dupont S, Piccolo S (2012) Transduction of mechanical and cytoskeletal cues by YAP and TAZ. Nat Rev Mol Cell Biol 13(9):591–600. [PubMed: 22895435]
34. Kassianidou E, Hughes JH, Kumar S (2017) Activation of ROCK and MLCK tunes regional stress fiber formation and mechanics via preferential myosin light chain phosphorylation. Mol Biol Cell:mbc.E17-06-0401.
35. Gupton SL, Waterman-Storer CM (2006) Spatiotemporal Feedback between Actomyosin and Focal-Adhesion Systems Optimizes Rapid Cell Migration. Cell 125(7): 1361–1374. [PubMed: 16814721]
36. Suvà ML, et al. (2014) Reconstructing and Reprogramming the Tumor-Propagating Potential of Glioblastoma Stem-like Cells. Cell 157(3):580–594. [PubMed: 24726434]
37. Sung CK, Li D, Andrews E, Drapkin R, Benjamin T (2013) Promoter methylation of the SALL2 tumor suppressor gene in ovarian cancers. Mol Oncol 7(3):419–427. [PubMed: 23273547]
38. Hermosilla VE, et al. (2017) Developmental SALL2 transcription factor: A new player in cancer. Carcinogenesis 38(7):680–690. [PubMed: 28430874]
39. Sung CK, Yim H (2015) The tumor suppressor protein p150Sal2 in carcinogenesis. Tumor Biol 36(2):489–494.
40. Zanconato F, et al. (2015) Genome-wide association between YAP/TAZ/TEAD and AP-1 at enhancers drives oncogenic growth. Nat Cell Biol 17(9): 1218–1227. [PubMed: 26258633]
41. Takada Y, Ye X, Simon S (2007) The integrins. Genome Biol 8(5). doi:10.1186/gb-2007-8-5-215.

42. Ramirez NE, et al. (2011) The α 2 β 1 integrin is a metastasis suppressor in mouse models and human cancer. J Clin Invest 121(l):226–237. [PubMed: 21135504]
43. Zutter MM, Mazoujian G, Santoro S a (1990) Decreased expression of integrin adhesive protein receptors in adenocarcinoma of the breast. Am J Pathol 137(4):863–870. [PubMed: 2221016]
44. Jovanović B, et al. (2014) Transforming growth factor beta receptor type III is a tumor promoter in mesenchymal-stem like triple negative breast cancer. Breast Cancer Res 16(4):R69. [PubMed: 24985072]
45. Su Z, et al. (2014) A comprehensive assessment of RNA-seq accuracy, reproducibility and information content by the Sequencing Quality Control Consortium. Nat Biotechnol 32(9):903–914. [PubMed: 25150838]
46. Symersky J, Osowski D, Walters DE, Mueller DM (2012) Oligomycin frames a common drug-binding site in the ATP synthase. Proc Natl Acad Sci U S A 109(35):13961–5. [PubMed: 22869738]
47. Cerniglia GJ, et al. (2015) The PI3K/Akt Pathway Regulates Oxygen Metabolism via Pyruvate Dehydrogenase (PDH)-Elalpha Phosphorylation. Mol Cancer Ther 14(8):1928–1938. [PubMed: 25995437]
48. Elstrom RL, et al. (2004) Akt Stimulates Aerobic Glycolysis in Cancer Cells. Cancer Res 64(11):3892–3899. [PubMed: 15172999]
49. Sarosiek KA, Ni Chonghaile T, Letai A (2013) Mitochondria: Gatekeepers of response to chemotherapy. Trends Cell Biol 23(12):612–619. [PubMed: 24060597]
50. Vlashi E, et al. (2011) Metabolic state of glioma stem cells and nontumorigenic cells. Proc Natl Acad Sci 108(38): 16062–16067. [PubMed: 21900605]
51. Vlashi E, et al. (2014) Metabolic differences in breast cancer stem cells and differentiated progeny. Breast Cancer Res Treat. doi:10.1007/s10549-014-3051-2.
52. Tung JC, et al. (2015) Tumor mechanics and metabolic dysfunction. Free Radic Biol Med 79:269–280. [PubMed: 25532934]
53. Zanotelli MR, et al. (2018) Regulation of ATP utilization during metastatic cell migration by collagen architecture. Mol Biol Cell 29(1): 1–9. [PubMed: 29118073]
54. Lyra-Leite DM, et al. (2017) Mitochondrial function in engineered cardiac tissues is regulated by extracellular matrix elasticity and tissue alignment. Am J Physiol Circ Physiol 313(4):H757–H767.
55. Bays JL, Campbell HK, Heidema C, Sebbagh M, DeMali KA (2017) Linking E-cadherin mechanotransduction to cell metabolism through force-mediated activation of AMPK. Nat Cell Biol 19(6): 724–731. [PubMed: 28553939]
56. Hu H, et al. (2016) Phosphoinositide 3-Kinase Regulates Glycolysis through Mobilization of Aldolase from the Actin Cytoskeleton. Cell 164(3):433–446. [PubMed: 26824656]
57. Tharp KM, et al. (2018) Actomyosin-Mediated Tension Orchestrates Uncoupled Respiration in Adipose Tissues. Cell Metab 27(3):602–615.e4. [PubMed: 29514068]
58. Ozawa S, et al. (2015) Glycolysis, but not Mitochondria, responsible for intracellular ATP distribution in cortical area of podocytes. Sci Rep 5. doi:10.1038/srep18575.
59. Carén H, et al. (2015) Glioblastoma Stem Cells Respond to Differentiation Cues but Fail to Undergo Commitment and Terminal Cell-Cycle Arrest. Stem Cell Reports 5(5):829–842. [PubMed: 26607953]
60. Berezovsky AD, et al. (2014) Sox2 promotes malignancy in glioblastoma by regulating plasticity and astrocytic differentiation. Neoplasia (United States) 16(3):193–206.
61. Carén H, Beck S, Pollard SM (2016) Differentiation therapy for glioblastoma – too many obstacles? Mol Cell Oncol 3(2):e1124174. [PubMed: 27308621]
62. Safa AR, Saadatzadeh MR, Cohen-Gadol AA, Pollok KE, Bijangi-Vishehsaraei K (2015) Glioblastoma stem cells (GSCs) epigenetic plasticity and interconversion between differentiated non-GSCs and GSCs. Genes Dis 2(2):152–163. [PubMed: 26137500]
63. Rammensee S, Kang MS, Georgiou K, Kumar S, Schaffer DV. (2017) Dynamics of Mechanosensitive Neural Stem Cell Differentiation. Stem Cells 35(2):497–506. [PubMed: 27573749]

64. Lee JY, et al. (2019) YAP-independent mechanotransduction drives breast cancer progression. Nat Commun 10:529. doi:10.1101/495499. [PubMed: 30705265]

65. Streitberger KJ, et al. (2014) High-resolution mechanical imaging of glioblastoma by multifrequency magnetic resonance elastography. PLoS One 9(10). doi: 10.1371/journal.pone.0110588.

66. Acerbi I, et al. (2015) Human breast cancer invasion and aggression correlates with ECM stiffening and immune cell infiltration. Integr Biol 7(10): 1120–1134.

67. Morfouace M, et al. (2012) Comparison of spheroids formed by rat glioma stem cells and neural stem cells reveals differences in glucose metabolism and promising therapeutic applications. J Biol Chem. doi: 10.1074/jbc.M111.320028.

68. Lee JP, Kassianidou E, MacDonald JI, Francis MB, Kumar S (2016) N-terminal Specific Conjugation of Extracellular Matrix Proteins to 2-Pyridinecarboxaldehyde Functionalized Polyacrylamide Hydrogels. Biomaterials 102:268–276. [PubMed: 27348850]

69. Schindelin J, et al. (2012) Fiji: an open-source platform for biological-image analysis. Nat Methods 9(7):676–682. [PubMed: 22743772]

70. Bioinformatics B FastQC: a quality control tool for high throughput sequence data. Available at: http://www.bioinformatics.bbsrc.ac.uk/projects/fastqc/.

71. Kim D, et al. (2013) TopHat2: accurate alignment of transcriptomes in the presence of insertions, deletions and gene fusions. Genome Biol 14(4):R36. [PubMed: 23618408]

72. Trapnell C, et al. (2012) Differential analysis of gene regulation at transcript resolution with RNA-seq. Nat Biotechnol 31. doi: 10.1038/nbt.2450.

73. Jiao X, et al. (2012) DAVID-WS: a stateful web service to facilitate gene/protein list analysis. Bioinformatics 28(13): 1805–6. [PubMed: 22543366]

Highlights

- Under self-renewing conditions, patient-derived glioblastoma tumor-initiating cells (TICs) have very similar transcriptional profiles on soft matrices and stiff matrices.
- Exposing TICs to the neural stem cell morphogen bone morphogenetic protein-4 (BMP4) sensitizes the TIC transcriptome to changes in matrix stiffness.
- Unexpectedly, genes related to oxidative phosphorylation are highly differentially expressed by TICs cultured on different matrix stiffnesses.
- Oxygen consumption and susceptibility to the ATP synthase inhibitor oligomycin are strongly influenced by differentiation state and matrix stiffness.

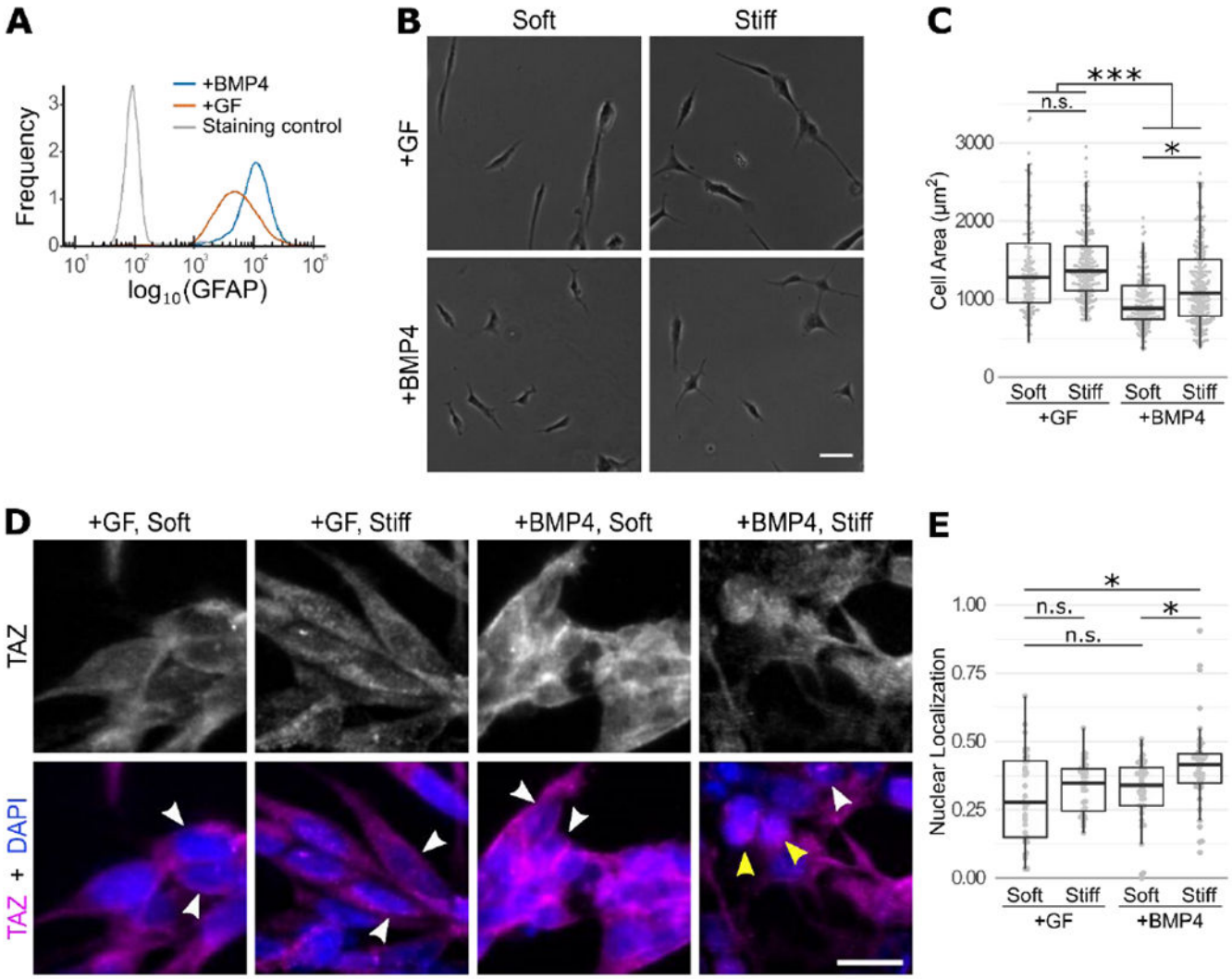

Figure 1:

BMP4 treatment elicits a pro-differentiation effect, and sensitizes cell spreading and TAZ (WWTR1) localization to substrate stiffness. (A) TICs cultured for 2 days on laminin-coated tissue culture plastic in self-renewing media (Neurocult enriched with EGF and FGF; "+GF") or BMP4-supplemented media (Neurocult with BMP4; "+BMP") were probed for GFAP and analyzed by flow cytometry. Representative curves from within a single experiment are shown. Cell counts as follows: +BMP4: 18,900 cells; +GF: 45,000 cells; staining control: 6000 cells. (C) Representative phase-contrast images of cells grown in growth factor-supplemented (GF) or BMP4-supplemented (BMP4) media on soft (200 Pa) or stiff (40 kPa) ECMs. Scale bar indicates 50 μm. (D) Quantification of cell area of cells cultured in GF- or BMP4-supplemented media on soft or stiff gels (n = 134, 207, 156, 232 respectively from left to right, collected from three independent experiments for each condition). Asterisks indicate significance as calculated with a Kruskal-Wallis one-way analysis of variance followed by a posthoc Kruskal-Dunn test with Holm's method for adjusting for multiple comparisons: * $p_{adj} < 0.05$, *** $p_{adj} < 0.001$, n.s. $p_{adj} > 0.05$. (E) Representative images of cells grown in GF- or BMP4-supplemented media on soft (200 Pa)

or stiff (40 kPa) gels stained for TAZ (WWTR1). Top row: TAZ channel. Bottom row: TAZ (magenta) merged with DAPI (blue). Scale bar indicates 5 μm. Arrows indicate cells with particularly prominent TAZ exclusion from (white arrows) or localization to (yellow arrows) the nucleus. (F) Quantification of immunofluorescence intensity of nuclear TAZ normalized to total TAZ intensity per field of view (n = 43, 48, 61 and 61 images respectively from left to right, collected from three independent experiments for each condition). This metric was selected since cell clumping precluded segmentation of individual cells grown on soft gels in BMP4-supplemented media. Asterisks indicate significance as calculated by a Kruskal-Wallis one-way analysis of variance followed by a posthoc Kruskal-Dunn test with Holm's method for adjusting for multiple comparisons: * $p_{adj} < 0.05$,, n.s,$p_{adj} > 0.05$.

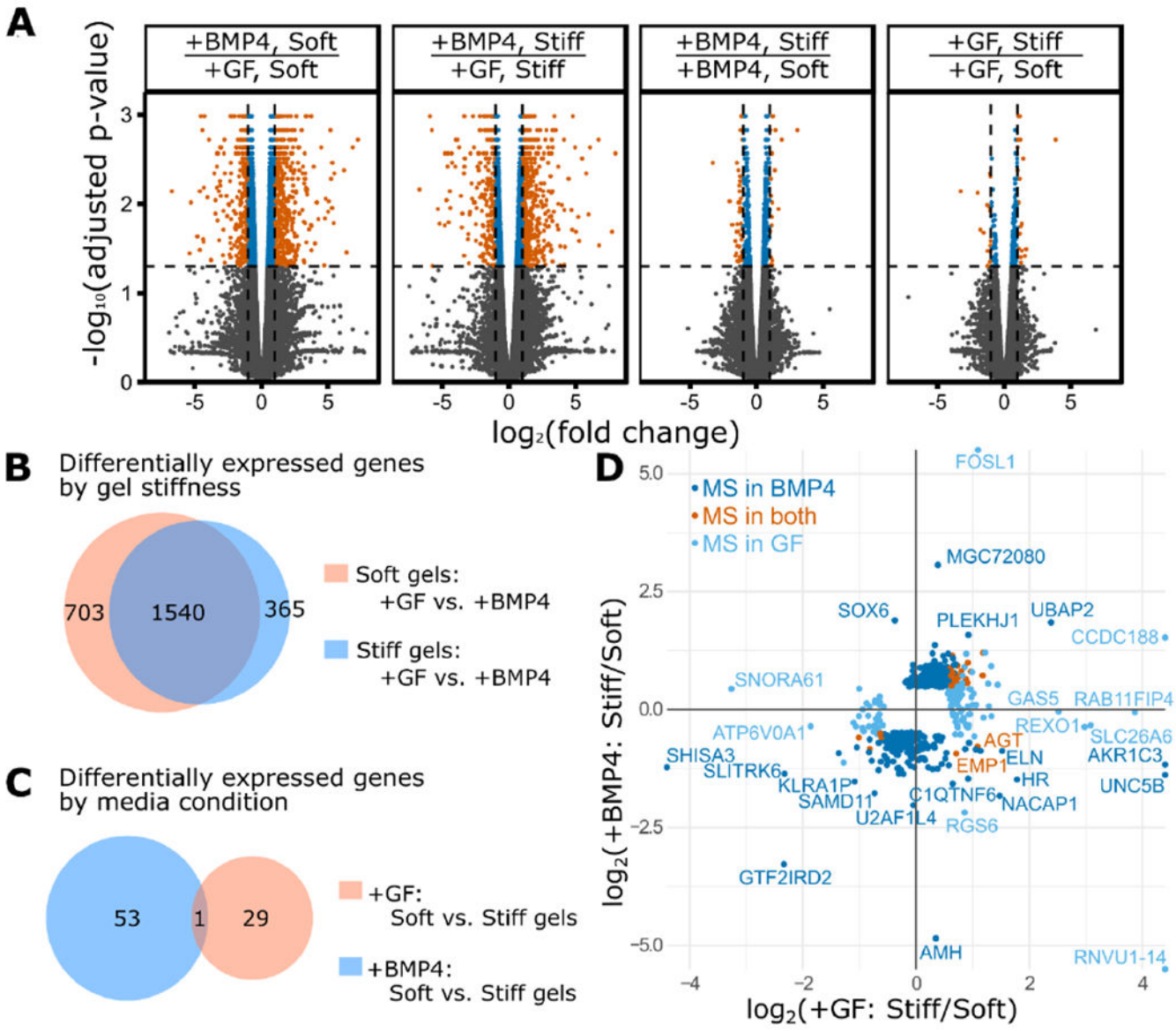

Figure 2:

Initial analysis of RNA sequencing results. (A) Volcano plots of false discovery rate (FDR) adjusted p-value versus fold-change for each comparison, with significantly differentially expressed (FDR < 0.05) genes highlighted in orange (fold-change > 2) or blue (fold-change ≤ 2). From left to right: BMP4-treated cells versus growth factor (GF)-treated cells on stiff (40-60 kPa) gels; BMP4-treated cells versus GF-treated cells on soft (0.1-0.25 kPa) gels; BMP4-treated cells on stiff versus soft gels; GF-treated cells on stiff versus soft gels. (B) Breakdown of number of genes significantly (FDR < 0.05, fold-change > 2) influenced by BMP4 treatment by relationship to substrate stiffness. (C) Breakdown of mechanosensitive genes, defined here as genes that are significantly differentially expressed (FDR < 0.05, fold-change > 2) on soft versus stiff gels. (D) Fold-change of mechanosensitive (MS) genes for BMP4-treated cells versus GF-treated cells, coded by whether they are significantly differentially expressed (FDR < 0.05) in both media conditions, or only significantly

differentially expressed in one of the treatment conditions. Gene names are shown for genes that show mechanosensitivity in either treatment condition with a fold change of at least $2^{1.5}$ and for the two genes that change their direction of mechanosensitivity.

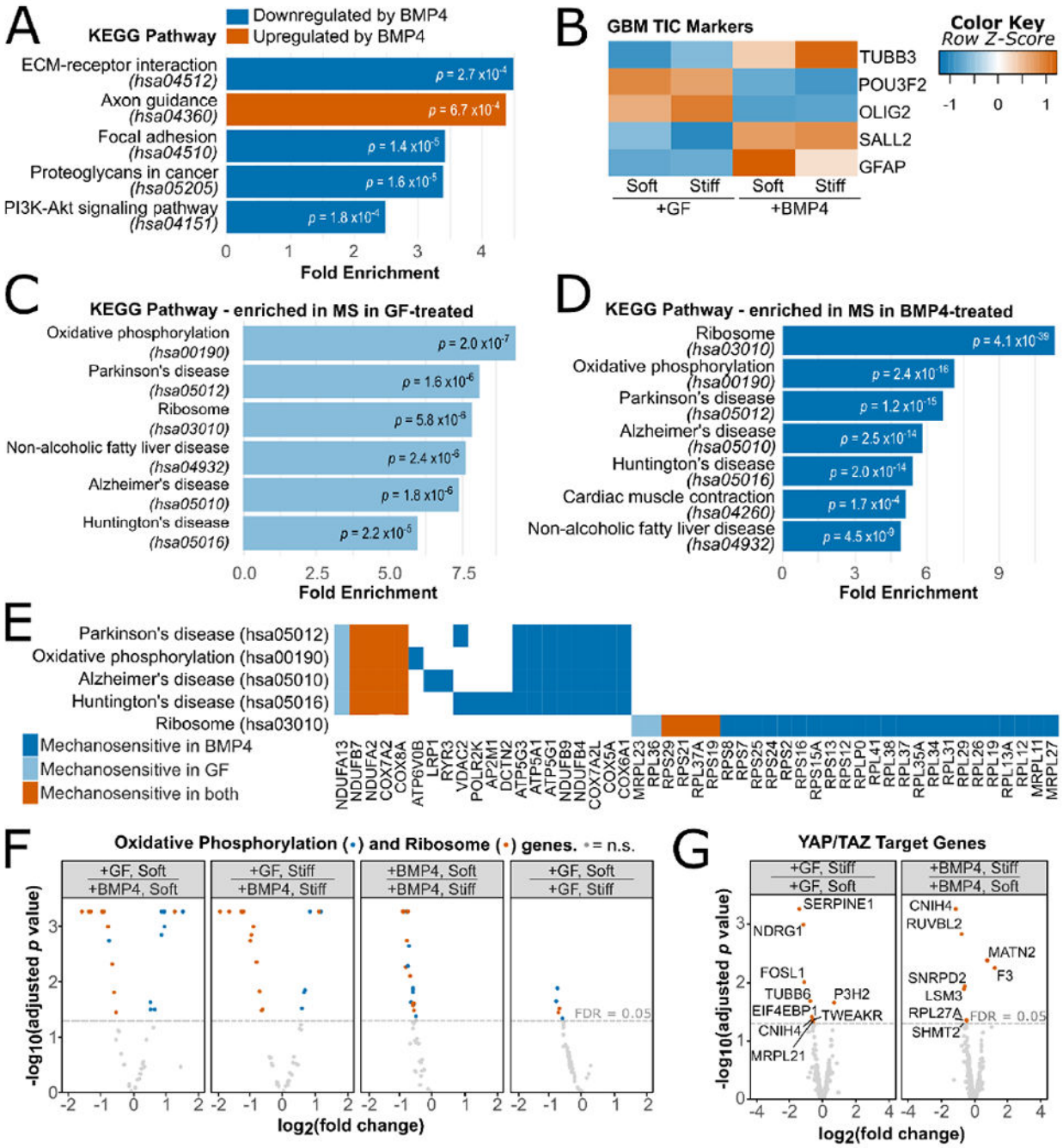

Figure 3:

Pathway analysis shows BMP4 signaling downregulates ECM communication and upregulates neural markers while stiffness cues influence ribosome proteins and oxidative phosphorylation genes. **(A)** KEGG pathway enrichment analysis for genes that are differentially expressed (FDR < 0.05) with a fold change of at least $2^{1.5}$ in response to BMP4 treatment for cells grown on either stiff or soft gels. The displayed *p* values are adjusted according to Benjamini, and all pathways with Benjamini $p < 0.001$ and with a fold enrichment > 2 are shown. **(B)** Heat map analysis showing genes associated with neural

stem cell differentiation (7) and GBM cancer stemness (38). Genes for which BMP4 significantly (FDR < 0.05) impacted transcription for cells grown on at least one of the two stiffnesses studied are indicated with an asterisk (*). **(C-D)** KEGG pathway enrichment analysis for genes that are differentially expressed (FDR < 0.05) in response to differences in substrate stiffness (mechanosensitive; MS) for cells cultured in **(C)** GF-enriched media or **(D)** BMP4-supplemented media. The displayed p values are adjusted according to Benjamini, and all pathways with Benjamini $p < 0.001$ and with a fold enrichment > 2 are plotted. **(E)** Stiffness-regulated genes belonging to the pathways identified in (C-D) color-coded by the conditions under which they are mechanosensitive to demonstrate degree of overlap. **(F)** Volcano plots for genes in the KEGG pathways hsa03010: Ribosomes and hsa:00190 Oxidative phosphorylation. **(G)** Volcano plots for YAP/TAZ targets as identified previously (32, 40), with gene names shown for significantly differentially expressed genes.

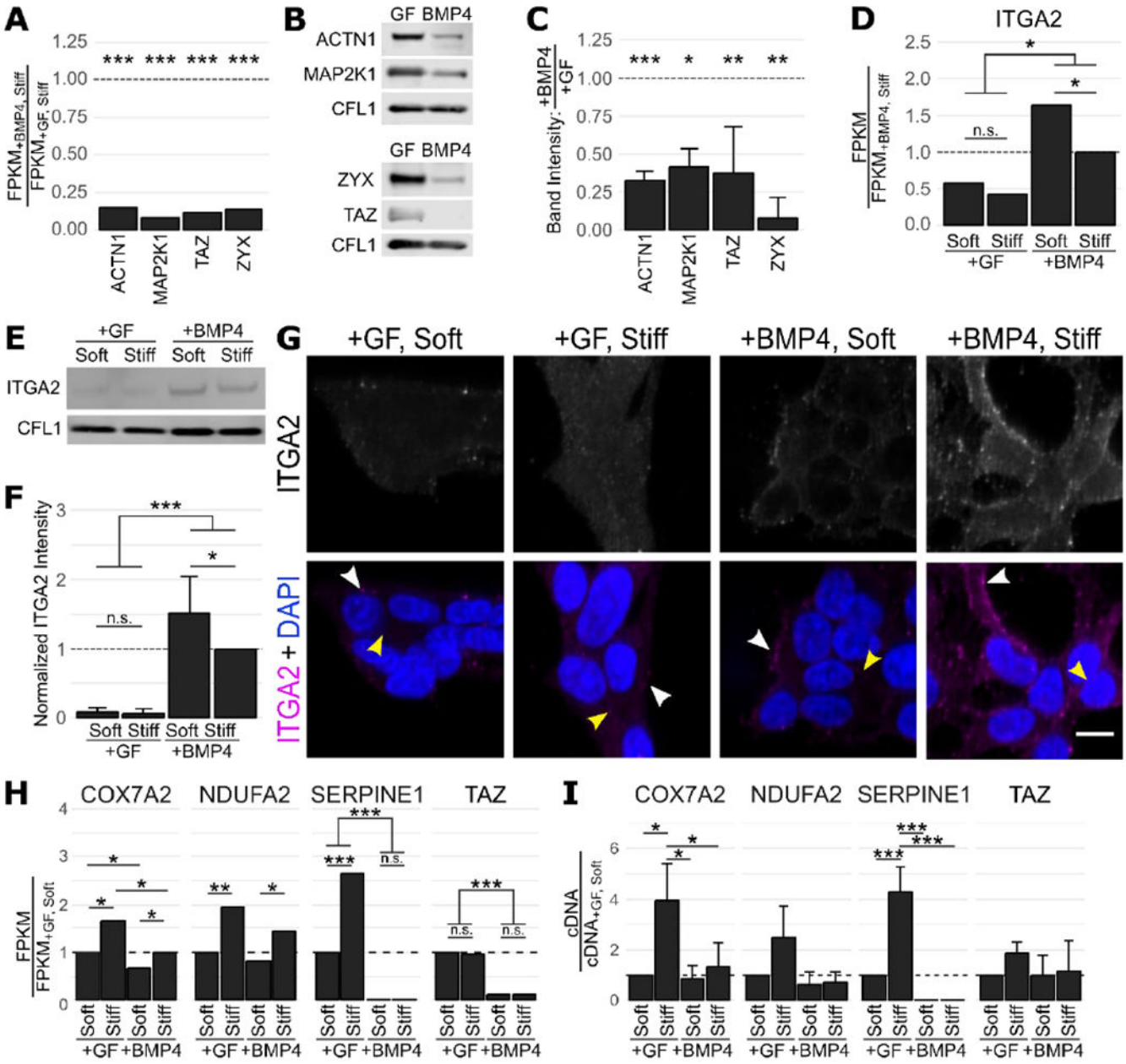

Figure 4:

RNA sequencing observations predict changes in protein level for genes altered by BMP4 treatment. (A) Replotting of RNA sequencing data of targets selected for immunoassay confirmation; ratio of FPKM for the BMP4-treated condition to the control GF-enriched condition for cells grown on stiff gels, with asterisks indicating FDR-adjusted p-value. (B) Representative western blots and (C) quantification for targets shown in (A). Lysates were collected from cells were grown on laminin-coated tissue culture plates for 7 days in either growth factor-enriched conditions (GF) or 100 ng/ml BMP4 (BMP4). Each blot was also probed for cofilin as a loading control. Band intensities were normalized first to cofilin, and then to the intensity of the GF-treated condition. Bars represent mean, error bars represent

standard deviation, and p-values were calculated by a Student's t-test (n = 4, 3, 5, 3; respectively, from left to right). (D) Replotting of RNA sequencing data for ITGA2, with asterisks indicating FDR-adjusted p-value. (E) Representative western blot and (F) quantification for ITGA2. Lysates were collected from cells grown on gels of the denoted stiffness for 7 days in the denoted media condition. Band intensities were normalized first to cofilin and then to the band intensity of the BMP4-treated cells cultured on stiff gels. Bars represent mean, error bars represent standard deviation and asterisks indicate statistically significant differences calculated with a one-way ANOVA followed by Tukey's range test (n = 7). (G) Representative images for cells probed for ITGA2. Arrowheads indicate areas with presence or absence of staining at cell periphery (white arrows) or cell-cell contact points (yellow arrows). (H) Replotting of RNA sequencing data of targets selected for rt-PCR confirmation; ratio of FPKM for each condition normalized to the GF-enriched cells grown on soft gels. (I) Relative mRNA expression compared to GF-enriched cells grown on soft gels, normalized to expression of RPS9, assayed by rt-PCR. Bars represent mean, error bars represent standard deviation, and p-values were calculated by a Student's t-test (n = 3 independent experimental replicates per condition and 2 technical replicates per experimental replicate). Lysates were collected from cells were grown on laminin-coated tissue culture plates for 7 days in either growth factor-enriched conditions (GF) or 100 ng/ml BMP4 (BMP4). n.s.: $p > 0.05$, *: $p < 0.05$, **: $p < 0.01$, ***$p < 0.001$.

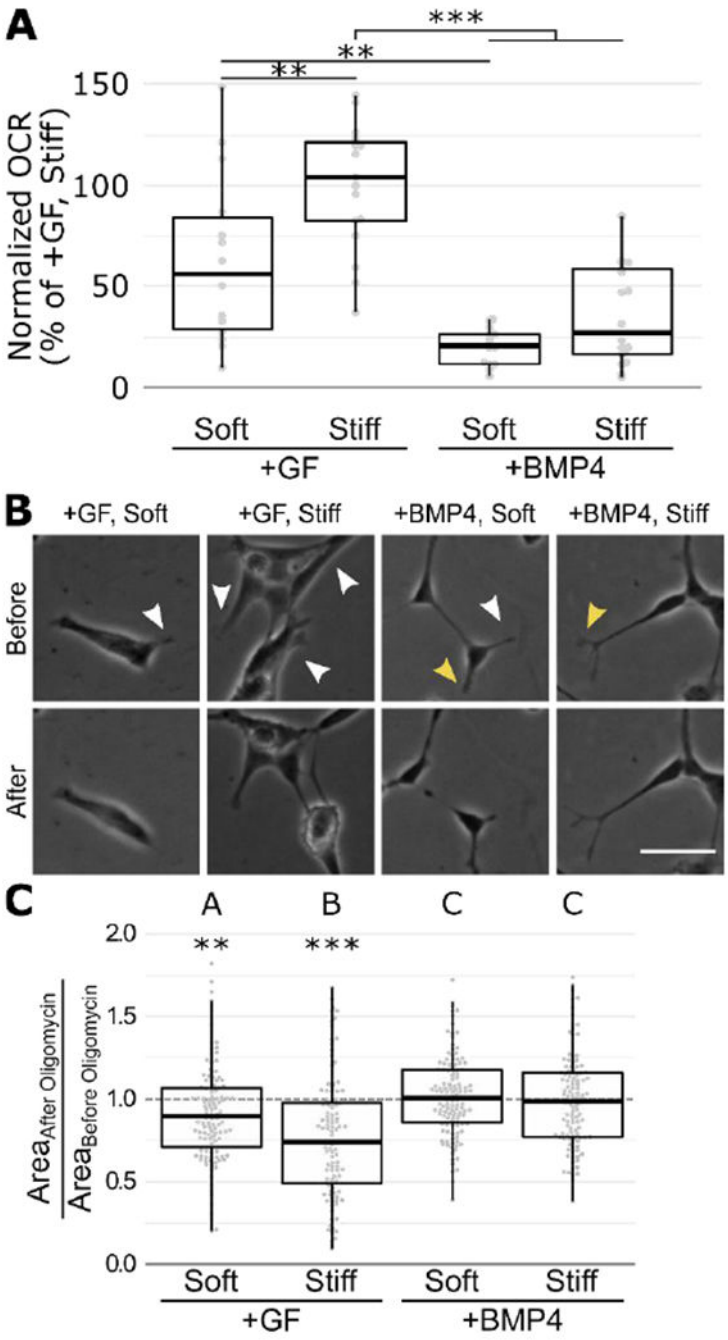

Figure 5:

Oxidative phosphorylation rates are dependent on stiffness and differentiation. **(A)** Basal oxygen consumption rate (OCR) for 50,000 cells, normalized to within-experiment GF-treated cells grown on stiff gels (n = 14, 17, 14, 18, respectively from left to right). Asterisks indicate significance as calculated from a one-way ANOVA with *p* values adjusted for multiple comparisons using Tukey's range test (n.s.: $p > 0.05$, ** $p < 0.01$, *** $p < 0.001$). **(B)** Representative images of TICs prior to and 30 minutes after addition of 5 μM oligomycin. White arrows indicate protrusions that retract after inhibition of ATP synthase,

yellow arrows indicate protrusions that showed extension after oligomycin treatment. **(C)** Quantification of cell area changes in response to oligomycin. A ratio of 1 indicates that a 30-minute incubation in 5 μM oligomycin produced no net change in cell area while a ratio of less than 1 indicates a decrease in area for that cell. Asterisks indicate ratios statistically distinct from 1, as determined by a 2-sided Mann Whitney U test (n.s.: $p > 0.05$, **: $p < 0.01$, *** $p < 0.001$). Letters indicate statistically distinct ($p_{adj} < 0.05$) distributions as calculated by a Kruskal-Wallis one-way analysis of variance followed by a post-hoc Kruskal Dunn test with Holm's method for adjusting for multiple comparisons, (n = 119, 113, 123, 113 cells per condition, respectively from left to right).